A modified resistance equation for modeling underwater spark discharge with salinity and high pressure conditions

Pengfei Zhao and Subrata Roy

Citation: Journal of Applied Physics **115**, 173301 (2014); doi: 10.1063/1.4874184
View online: http://dx.doi.org/10.1063/1.4874184
View Table of Contents: http://scitation.aip.org/content/aip/journal/jap/115/17?ver=pdfcov
Published by the AIP Publishing

A modified resistance equation for modeling underwater spark discharge with salinity and high pressure conditions

Pengfei Zhao and Subrata Roy[a)]
Applied Physics Research Group, Department of Mechanical and Aerospace Engineering, University of Florida, Gainesville, Florida 32611, USA

(Received 1 March 2014; accepted 17 April 2014; published online 2 May 2014)

This work investigates the performance of underwater spark discharge relating to bubble growth and decay under high pressure and with salinity conditions by introducing a modified form of the resistance equation. Here, we study salinity influence on circuit parameters by fitting the experimental data for which gap resistance is much larger in conductive water than in dielectric water. Accordingly, the resistance equation is modified by considering the influence of both plasma and its surrounding liquid. Thermal radiation effect of the bubble is also studied by comparing two different radiation models. Numerical results predict a larger bubble pressure for saline water but a reduced size and a smaller bubble cycle at a greater water depth. Such study may be useful in many saltwater applications, including that for deep sea conditions. © *2014 AIP Publishing LLC*. [http://dx.doi.org/10.1063/1.4874184]

I. INTRODUCTION

Since its inception nearly ninety years ago,[1] underwater spark discharges were investigated and employed in various applications. Examples include underwater acoustic source in deep ocean oil prospecting[2] and minesweeping applications,[3] underwater plasma source in advanced water sterilization method,[4,5] powerful underwater shock wave source in extracorporeal lithotripsy[6] and oil well dredging,[7] and active reaction source in water treatment.[8,9] In recent decades, many related experiments[10–14] had been designed for understanding the mechanism of this complex physical phenomenon. Based on these experimental results some theoretical and empirical models[15–19] have also been developed to predict the shock wave pressure, electro-acoustical efficiency, chemical reaction, ionization, and associated plasma processes.

The brief (∼microseconds) mechanism of underwater spark discharge can be divided into two parts. At the beginning of the first part, when the capacitor, charged with a high voltage, is connected to the discharge circuit, a high electric field ($E > MV/m$) is formed in the liquid channel between the two submerged electrodes. Immediately after, in a non-conducting liquid, such as pure water, a low density channel is formed between the electrodes due to several possible mechanisms, such as small void generation by electrostatic repulsion and electrostriction force,[11] or the presence of a seed gas bubble inside the gap.[20] Then, an electrical spark discharge is initiated within this channel due to high E-field. In a conducting liquid like seawater, this high electric field generates a large current, which directly goes through the liquid and forms an evaporation channel in it. During the second part, both conducting and non-conducting liquids violently release the energy stored within the capacitor through the formed channel as the Joule heating effect evaporates the liquid, and eventually dissociates and/or ionizes its constituents.[6] Consequently, the channel with high pressure and temperature expands rapidly in all directions as a spherical "bubble." This bubble wall starts oscillating due to compressibility effect generating sequential spherical acoustic compression waves. In summary, the first part of underwater spark discharge process is the bubble initiation due to a high electric field, and the second part is the pulsed energy release, bubble expansion and oscillation. Importantly, the bubble characteristics are determined from the second part, which we model and simulate in this paper.

Since the underwater spark discharges are frequently used in conducting liquid such as seawater, the salinity of water, which affects the conductivity, should influence the rate of energy release in the water, and thus influences the bubble growth. There are a few experimental studies that show advantages of spark discharge in a conducting liquid. For example, Bourlion *et al.*[6] reported no latency period before discharge and a significant reduction on the wear of the electrodes in electro-conductive solution compared to that in pure (dielectric) water. However, the underlying mechanism explaining the influence of salinity on the bubble growth is yet to be reported. Also, many applications of underwater spark discharge are at great ocean depths that generate extremely large ambient pressures. This area of research remains largely unexplored, necessitating a fundamental study of bubble characteristics under these extreme conditions.

In this paper, we present theoretical simulations of the bubble generated by underwater spark discharge using a circuit model with salinity and large ambient pressure effects, and analyze their influencing mechanisms. Furthermore, the effects of circuit parameters are also investigated.

II. THEORETICAL ANALYSIS

A. Assumptions

The following assumptions are made for the theoretical model: (1) The bubble is a symmetric sphere. (2) The effects

[a)]Email: roy@ufl.edu. URL: http://aprg.mae.ufl.edu/roy/.

of gravity are negligible. (3) The pressure and temperature inside the bubble are uniformly distributed. (4) The compressibility of water only affects the outside of the bubble. (5) Thermal effects of water are negligible outside the bubble. (6) The plasma inside the bubble is in local thermal equilibrium (LTE).

Assumption (1)–(3) are made to simplify the problem to a zero dimensional (0-D) model. Assumption (4) is made due to the fact that the bubble generated by spark discharge grows with a high wall velocity (>transonic). Consequently, thermal conduction in this fast process can be neglected,[21] which is assumption (5). Finally, assumption (6) is made according to the plasma parameters obtained in the experiment.[6] The temperature and electron density of plasma inside the bubble can reach up to 5 eV and 10^{28} m^{-3}, respectively; for which, the lifecycle of the plasma is several milliseconds. In order to be considered as LTE plasma, this transient plasma must fulfill two criteria[22]

$$N_e \geq 10^{23}\left(\frac{kT}{E_H}\right)^{1/2}\left(\frac{E_2-E_1}{E_H}\right)^3[\mathrm{m}^{-3}], \tag{1}$$

$$\tau \approx \frac{1.15\times 10^7 N^+}{f_{21}N_e(N^++N)}\left(\frac{E_2-E_1}{E_H}\right)\left(\frac{kT}{E_H}\right)^{1/2}\exp\left(\frac{E_2-E_1}{kT}\right)[\mathrm{s}], \tag{2}$$

where N_e is the electron density, k is the Boltzmann constant, T is temperature, E_H is the first ionization energy of hydrogen (or oxygen) atom, E_n is the nth electron state energy, τ is the relaxation time, f_{21} is the absorption oscillator strength, and N^+ and N are the number density of ions and neutral atoms, respectively. In Ref. 22, it was shown that for this plasma $N_e \geq 10^{24}$ m^{-3} and $\tau < 10^{-9}$ s which satisfy the LTE criteria from Eqs. (1) and (2).

B. Bubble model

In this work, we used an effective model published by Lu *et al.*[15] with some modification to simulate the bubble variation. According to the assumptions listed above, the 0-D bubble model of underwater spark discharge should consider water compressibility and neglect thermal effects on the surrounding water. So, the Kirkwood–Bethe approximation of bubble equation of motion, as an effective model, is employed to simulate bubble oscillation process

$$\left(1-\frac{1}{C}\frac{\mathrm{d}R}{\mathrm{d}t}\right)R\frac{\mathrm{d}^2R}{\mathrm{d}t^2}+\frac{3}{2}\left(1-\frac{1}{3}\frac{1}{C}\frac{\mathrm{d}R}{\mathrm{d}t}\right)\left(\frac{\mathrm{d}R}{\mathrm{d}t}\right)^2 = \left(1+\frac{1}{C}\frac{\mathrm{d}R}{\mathrm{d}t}\right)H+\left(1-\frac{1}{C}\frac{\mathrm{d}R}{\mathrm{d}t}\right)\frac{R}{C}\frac{\mathrm{d}H}{\mathrm{d}t}. \tag{3}$$

In Eq. (3), H, the specific enthalpy, and C, the speed of sound, are the properties of liquid attaching the bubble, and R is the radius of the bubble. Since thermal effects are neglected in the water outside the bubble, explicit expressions for C and H can be derived by using the modified Tait equation of state[23]

$$\frac{p+B}{p_\infty+B}=\left(\frac{\rho}{\rho_\infty}\right)^n, \tag{4}$$

where p and ρ are the pressure and density of liquid attaching the bubble, p_∞ and ρ_∞ represent the pressure and density of water in the undisturbed region far from the bubble. The constants $B = 3.04913\times 10^8$ Pa and $n = 7.15$ are based on reasonable matching with the experimental pressure-density relation of water in the pressure range up to 10 GPa.[24]

Since the bubble wall is an interface of water and vapor, there is a difference between pressures on both sides of the wall due to normal stresses, which is

$$p_B(t)=p_i(t)-\frac{1}{R}\left(2\sigma+4\mu\frac{\mathrm{d}R}{\mathrm{d}t}\right). \tag{5}$$

Here, p_B (t) and p_i (t) are the pressures on the liquid side and vapor side of the interface, respectively, σ is the liquid-vapor surface tension, and μ is the viscosity of the liquid. However, the pressure difference (10^5 Pa) caused by surface tension and liquid viscosity is much less than the internal pressure (10^8 Pa) generated by spark discharge. So, this difference can be neglected and p is used to represent the pressure on both sides of the bubble wall in the rest of this paper.

Unlike arc discharges, which generally keep the plasma channel connecting the electrodes for longer periods and consume large amount of energy, spark discharges use less energy and only produce transitory conductive channels that bridge the gap between the electrodes.[10] Bubble pressure can be calculated using ideal gas model with contributions from all particles inside the bubble

$$p=\frac{kTN\eta(N,V,T)}{V}, \tag{6}$$

where k is the Boltzmann constant, T is the temperature of plasma, N is the number of equivalent whole water molecules in the bubble, $\eta(N, V, T)$ is the ratio of the number of all particle species to N (such that $N\eta$ is the total particle number in the bubble), and V is the bubble volume which is expressed by the bubble radius R.

In order to derive the expression for temperature, T, the time derivative of the internal energy, E, is needed

$$\frac{\mathrm{d}E}{\mathrm{d}t}=\left(\frac{\partial E}{\partial N}\right)_{V,T}\frac{\mathrm{dN}}{\mathrm{d}t}+\left(\frac{\partial E}{\partial V}\right)_{N,T}\frac{\mathrm{dV}}{\mathrm{d}t}+\left(\frac{\partial E}{\partial T}\right)_{N,V}\frac{\mathrm{dT}}{dt}. \tag{7}$$

Since the bubble here is an open system, a different expression for the energy balance with energy flow can be derived from the first law of thermodynamics

$$\frac{\mathrm{d}E}{\mathrm{d}t}=q-p\frac{\mathrm{d}V}{\mathrm{d}t}+\left(\frac{\partial E}{\partial N}\right)_{V,T}\frac{\mathrm{d}N}{\mathrm{d}t}, \tag{8}$$

$$q=q_{input}-(1-\gamma)q_{rad}-q_m, \tag{9}$$

where q_{input} is the energy flow injected in the spark between the electrodes from circuit, q_{rad} is the heat flow due to radiation, γ is the fraction of the radiant energy absorbed by the bubble interface for evaporation, q_m is the energy flow that

includes evaporation, condensation, and heating due to the mass exchange through the interface. By combining Eqs. (7) and (8), the expression for T is

$$\left(\frac{\partial E}{\partial T}\right)_{N,V}\frac{\mathrm{d}T}{\mathrm{d}t}=q-\left[p+\left(\frac{\partial E}{\partial V}\right)_{N,T}\right]\frac{\mathrm{d}V}{\mathrm{d}t}. \tag{10}$$

In order to derive the expression of internal energy, E, needed for solving Eq. (10), the analysis of the internal content of the bubble should be predetermined. Inside the bubble, we can simply consider reactions due to high temperature and pressure, dissociation of water molecules into separated atoms and ionization of hydrogen and oxygen atoms. Since we have assumed that the plasma inside bubble is in LTE, the dissociation and ionization processes must be in equilibrium. For such an equilibrium, let S be the probability of the state that gas of i species with N_i particles has in a given volume, V. The probability for dissociation is

$$S=\Pi_i\frac{Z_i^{N_i}}{N_i!}=\frac{Z_H^{N_H}}{N_H!}\frac{Z_O^{N_O}}{N_O!}\frac{Z_{H_2O}^{N_{H_2O}}}{N_{H_2O}!}, \tag{11}$$

where Z_i is the partition functions for each particle species i. For hydrogen and oxygen atoms, the expression is

$$Z_i=g_iV\left(\frac{2\pi m_ikT}{h^2}\right)^{3/2}, \tag{12}$$

where h is the Planck constant, g_i is the degeneracies of the particle i, and m_i is the mass of the particle i. The partition functions for water molecules are identical, except there the binding energy, D, is included.

$$Z_{H_2O}=g_{H_2O}V\left(\frac{2\pi m_{H_2O}kT}{h^2}\right)^{3/2}\exp\left(\frac{D}{kT}\right). \tag{13}$$

From dissociation of N water molecules, we have

$$N_H=2N_O, \tag{14}$$

$$N_{H_2O}=N-N_O. \tag{15}$$

Then, taking the derivative of the natural log of Eq. (11) and using Stirling's approximation for $N, N_i \gg 1$, we can get the dissociation equilibrium expression

$$\frac{\mathrm{d}(\ln S)}{\mathrm{d}N_O}=2\ln Z_H+\ln Z_O-\ln Z_{H_2O}-2\ln(N_H)-\ln N_O+\ln(N_{H_2O})=0, \tag{16}$$

$$\frac{N_H^2N_O}{N_{H_2O}}=\frac{Z_H^2Z_O}{Z_{H_2O}}=\frac{V^2g_H^2g_O}{g_{H_2O}}\left(\frac{m_O}{m_{H_2O}}\right)^{3/2}\left(\frac{2\pi m_HkT}{h^2}\right)^3\exp\left(-\frac{D_{H_2O}}{kT}\right). \tag{17}$$

For ionization equilibrium, the ionization potential is the same for both hydrogen oxygen atoms. So, only the ionization equilibrium equation of the hydrogen atom is calculated for both atom ionization processes

$$\frac{N_{H^+}N_e}{N_H}=\frac{Vg_{H^+}g_e}{g_H}\left(\frac{m_{H^+}}{m_H}\right)^{3/2}\left(\frac{2\pi m_ekT}{h^2}\right)^{3/2}\exp\left(-\frac{I_1}{kT}\right), \tag{18}$$

where I_1 is the first ionization potential of hydrogen (or oxygen) atom. Now the internal energy, E, can be derived from Eqs. (17) and (18) as

$$E=N\left[(1-\alpha_1)\varepsilon_{H_2O}+\alpha_1D+3\alpha_1(1+\alpha_2)\varepsilon+3\alpha_1\alpha_2I_1\right], \tag{19}$$

where α_1 and α_2 are the degree of dissociation and the degree of ionization which can be easily calculated from equilibrium equations, and $\varepsilon_{H_2O}=3kT$ and $\varepsilon=3/2kT$ are internal energies for water molecule and all other particle species, respectively. The particle-molecule ratio, η, can be expressed as

$$\eta(N,V,T)=1+2\alpha_1+3\alpha_1\alpha_2. \tag{20}$$

Due to the high temperature of the constituents inside the bubble, the thermal radiation also needs to be considered in underwater spark discharge plasmas. Furthermore, this radiation will strongly interact with the charged particles inside the bubble. So, a realistic radiation model[15] considering optical thickness of the participating medium should be employed. The radiation energy flow rate can be calculated by

$$q_{rad}=4\pi R^2\int_0^\infty \pi I_{vp}\left\{1-\frac{1}{2\tau_v}\left[1-(1+2\tau_v)e^{-2\tau_v}\right]\right\}dv. \tag{21}$$

where I_{vp} is the energy flux of blackbody radiation and τ_v is the spectral optical thickness of the spherical bubble.

Mass exchange at the bubble wall plays a very important role as bubble properties vary. According to gas dynamic theory[25] and radiant evaporation, the mass flow rate of water, $\dot{m}$, and corresponding energy flow rate, q_m, can be expressed as

$$\dot{m}=\frac{4\pi R^2\alpha_M}{\sqrt{2\pi R_v}}\left(\frac{p^*}{\sqrt{T_l}}-\Gamma\frac{p}{\sqrt{T}}\right)+\frac{\gamma q_{rad}}{c_l(T_{ph}-T_l)+l}, \tag{22}$$

$$q_m=\dot{m}\left(c_l(T_{ph}-T_l)+l+\int_{T_{ph}}^{T}c_p(T')\mathrm{d}T'\right). \tag{23}$$

In Eq. (22), the first term is due to gas dynamic, where α_M is the accommodation coefficient for evaporation or condensation (assumed constant), equal to the ratio of vapor molecules sticking to the phase interface to those impinging on it, p is the actual vapor pressure, p^* is the equilibrium vapor pressure, T and T_l are the temperatures of the vapor and the liquid at the phase interface, respectively, and R_v is the gas constant of the vapor. The deviation of the velocity distribution from a Maxwellian distribution is described by the

factor Γ, which is equal to unity for equilibrium conditions.[24] Second term is radiant evaporation mass flow, where T_{ph} is the phase change temperature of water, c_l is the liquid specific heat capacity at constant pressure, and l is the latent heat of evaporation or condensation. In Eq. (23), $c_p(T)$ is the vapor specific heat capacity at constant pressure. The equilibrium vapor pressure can be calculated from Clausius-Clapeyron equation as[24]

$$p^* = p_c \exp\left[\frac{L}{R_v T_c}\left(1 - \frac{T_c}{T_i}\right)\right], \tag{24}$$

where T_c and p_c are the temperature and pressure at the critical point, for water 647.096 K and 2.206×10^7 Pa,[24] respectively. The specific heat at constant pressure can be expressed as

$$c_p(T) = \frac{1}{N m_{H_2O}}\left(\frac{\partial E}{\partial T}\right)_{N,V} + R_v. \tag{25}$$

Note, the time derivative of water molecule number can be expressed as

$$\frac{\mathrm{d}N}{\mathrm{d}t} = \frac{\dot{m}}{m_{H_2O}}. \tag{26}$$

C. Circuit model

The circuit of the power system is shown Fig. 1 (similar power systems are used in Refs. 6 and 15). This circuit includes two function sections, charge section and discharge section, sharing a capacitor. In the beginning of each pulse cycle, power source charges the capacitor to high voltage via transformer in the charge section. When spark gap switch is triggered, a high energy pulse is generated from discharging the capacitor and ignite underwater spark between two underwater electrodes. Then bubble is generated and oscillated as described. In this paper, the electrodes are 2 mm in diameter and the gap between electrodes is set as 0.2 mm.

During the discharging period, the bubble of plasma can be simply treated as a resistor. Thus, the discharge section becomes a series RLC circuit. So, we can use series RLC model to simulate this section

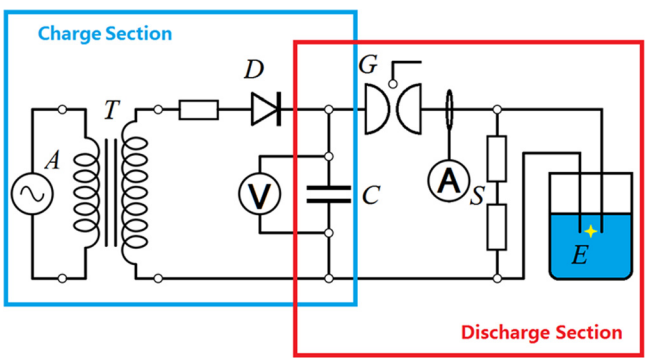

FIG. 1. Circuit of experiment setup, A is A/C power source, T is transformer, D is diode, C is the capacitor, G is spark gap switch, S is safety resistance, and E is underwater spark.

$$L\frac{di}{dt} + \Omega_{total} i + \frac{1}{C}\int_{t_0}^{t} i dt' - V_C(t_0) = 0 \tag{27}$$

In Eq. (27), L is the inductance of this section, $\Omega_{total} = \Omega_c + \Omega_g$ is the total resistance in this section, including both circuit resistance Ω_c and gap resistance Ω_g, i is the current, C is the capacitance, and V_C represents the voltage on the capacitor. Then, the input power can be determined as

$$q_{input} = i^2 \Omega_g \tag{28}$$

Since the two resistances are the only power consumption devices in the circuit and circuit resistance remains constant, the input energy is related to the gap resistance.

III. RESULTS AND DISCUSSION

A. Salinity analysis

Salinity influences the electrical conductivity of the liquid. Thus, it is very important in the electrical breakdown of water and the subsequent thermal and hydrodynamic phenomena. The ratio of electrical permittivity to conductivity in liquid, ε_l/σ_l, i.e., the Maxwell relaxation time is the time scale which characterizes the charge relaxation due to Ohmic conduction, and for a very short energy pulse relative to this relaxation time the fluid behaves as a dielectric.[10]

Bourlion *et al.*[6] presented voltage and current curves for both pure and saline water conditions. They used sodium chloride aqueous solution with concentration of 100 g/l, which can be convert to electrical conductivity of 14.29 S/m. For pure water discharge, after a random latency period, under-damped discharge ignites to high oscillating current. In saline water case, current curve is aperiodic, which indicates that the discharge is close to critically damped. From this phenomenon, one can imply that the resistance during the saline water discharge is higher than the resistance during the pure water discharge.

The larger gap resistance for saline water can be also explained by the mechanism in the first part of underwater spark. For dielectric liquid, such as pure water, since the liquid resistance is very high, even high electric potential cannot penetrate through. Then, a low density liquid channel is generated by high electric field in the gap between electrodes. Therefore, a random latency period[6] may appear in this case due to the channel formation process. Electrical discharge initiated in the channel evaporates and then ionizes the liquid into plasma, which become a low conductivity channel for releasing stored energy. For conductive liquid, this high electric field directly moves charged particles in the liquid to release energy bypassing the formation of a low density channel. Subsequently, the liquid evaporates, and eventually ionizes, due to Joule heating. Thus, relatively higher resistance in this case can be explained as heavier charged particles in comparison with the case of pure water (dielectric liquid). Furthermore, it can be foreseen that there must be a threshold condition connects these two typical cases describe above.

In summary, gap resistance during under water discharge contains two parts, one is the resistance of plasma

channel, and the other is the resistance of surrounding liquid. The expression of plasma channel resistance can be modified from[26] by adding energy forming pre-discharge channel to the internal energy. The resistance for surrounding liquid can be calculated from liquid resistance before discharge and the bubble radius. When bubble expands, the surrounding resistance will increase in proportion to the radius. That is, due to the path between electrodes through liquid directly relates to the radius when bubble exists. Then the gap resistance can be represented as modified plasma channel resistance parallel with surrounding liquid resistance (Fig. 2)

$$\frac{1}{\Omega_g} = \frac{1}{\Omega_{pl}} + \frac{1}{\Omega_{liq}} \tag{29a}$$

In Eq. (29), Ω_{pl} and Ω_{liq} can be represented as

$$\Omega_{pl} = \left(\frac{A_{pl} l_g^2}{E + E^*}\right), \quad \Omega_{liq} = A_{liq}\Omega_0, \quad \text{where}$$
$$A_{liq} = \begin{cases} 1 \ \text{for} R \le l_g \\ \dfrac{R}{l_g} \ \text{otherwise,} \end{cases} \tag{29b}$$

where A_{pl} is a constant which characterize the content of the spark channel, l_g is the gap length, E^* is the energy forming pre-discharge channel under dielectric liquid, and Ω_0 represents the liquid resistance before discharge which can be calculated from solving the Poisson equation according to the electrodes geometry.

We solve the Poison's equation according to the geometry of the experimental setup. The results of electrical potential and electrical field are shown in Fig. 3. Then, the equivalent resistance of the saline water can be calculated by

$$\Omega_0 = \frac{V_g}{I_g}, \quad \text{where} \, I_g = \int_0^R \sigma_s E_{field}(2\pi r) dr. \tag{30}$$

Here, $V_g = 1$ V denotes voltage applied between two electrodes, I_g is the current pass through the gap, σ_s is the saline water conductivity, and the integration is along the $Y = 0$ line. For saline water case described above, the gap resistance is calculated as 2000 mΩ. After getting all parameter required from Eq. (29), the current curves can be simulated

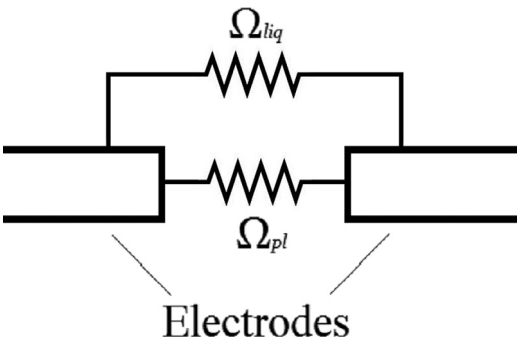

FIG. 2. Gap resistance model including the plasma resistance, Ω_{pl}, and the surrounding liquid resistance, Ω_{liq}.

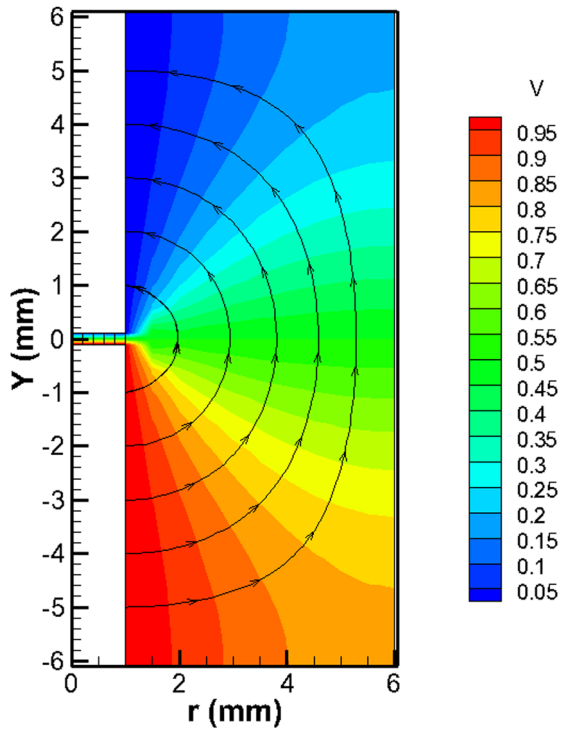

FIG. 3. The electric potential in the experimental setup[6] normalized by the applied voltage (V_g) with the electric field line overlay (only the symmetric half is shown).

using the model. In Fig. 4, it can be seen that the numerical simulation and experimental data fit very well with each other.

B. Simulation results

In this paper, five different cases are numerically simulated for studying the underlying influences of salinity and pressure. For numerical simulations of all cases, initial conditions and parameters are selected and validated according to experimental work by detecting pressure pulse generated by the spark discharge[15]

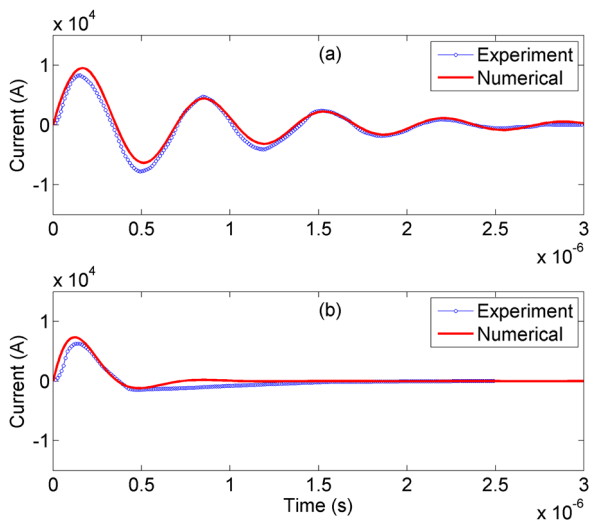

FIG. 4. Comparison between numerical simulation and experimental data from[6] (a) unsalted case and (b) salted case (with 100 g/l salt).

TABLE I. Water properties for all cases.[27]

	Salinity (g/l)	Temperature (°C)	Ambient pressure (Pa)	Density (kg/m^3)	Conductivity (S/m)	Ω_0 (Ω)
Unsalted water	N/A	20	1.01×10^5	998.21	N/A	Inf
Salted water	100	20	1.01×10^5	1074.05	14.29	2
Seawater (average)	35	20	1.01×10^5	1024.75	4.79	5.97
Deep sea (500 m)	35	10	5×10^6	1029.32	3.81	7.50
Deep sea (1000 m)	35	5	1×10^7	1032.38	3.35	8.54

$$p_{ini} = 2p_\infty, \quad T_{ini} = 400\,\mathrm{K}, \quad \frac{dR}{dt} = 6^{m/s}, \tag{31a}$$

$$\gamma = 0.2, \quad \alpha_M = 10^{-4}. \tag{31b}$$

Based on the experimental setup,[6] the following circuit parameters are utilized:

$$C = 100\,\mathrm{nF}, \quad L = 115\,\mathrm{nH}, \quad V_0 = 14.5\,\mathrm{kV}, \quad \Omega_c = 50\,\mathrm{m}\Omega. \tag{32}$$

In the latency period of unsalted case, the capacitor voltage decrease to 13.5 kV. So, the initial voltage of unsalted case is set to 13.5 kV.

The water properties for all cases are listed in Table I. The gap resistances for unsalted water and salted water case are calculated from fitted value. While the gap resistance for all seawater cases is calculated from the conductivity ratio between themselves and salted case. The seawater salinities and temperatures are the average values.

1. Salinity study

For salinity study, all properties during bubble expansion and oscillation process of all atmospheric cases are plotted together for comparison in Figs. 5–7. In order to compare the differences, the time axis of each case is plotted in logarithmic scale and is normalized according to the first bubble oscillation cycle period. The first cycle periods of all 3 cases are shown in the legend of Fig. 5(a) in parentheses. Note that the first cycle period for unsalted case does not include the random latency period. Similar first cycle periods are also observed in salinity studies. Several nanoseconds after the channel formation, the bubble grows rapidly till it reaches to a maximum in about 2 ms. This is followed by a slightly slower decay phase of the bubble radius that ends at about 3.5 ms.

Comparison of bubble radii is plotted in Fig. 5(a). As shown in the legend, the first bubble cycle periods are 3.45 ms, 3.61 ms, and 3.71 ms for unsalted, salted, and seawater cases, respectively. First cycle periods of all 3 cases are close to each other. Similarly, the maximum radii for unsalted (1.836 cm), salted (1.923 cm), and seawater (1.948 cm) cases are also very close. Furthermore, after first expansion, the bubble shrinks to a smaller size due to liquid compressibility. Although the bubble radii are almost identical for all three cases, the maximum wall velocities of the bubble shown in Fig. 5(b) vary with salinity differences. Saline water cases tend to have higher wall velocity in the beginning stage of the discharge. Furthermore, the trend of wall velocity is the same as that of pressure shown in Fig. 5(c). The velocity of bubble wall is in the transonic range of water and the pressure is in GPa level. Combination of the velocity and pressure, the spark discharge bubble can generate powerful acoustic wave.

Fig. 6(a) shows the instantaneous input power to the bubble from the power circuit. The periodic decreasing curve of unsalted case implies an under-damped discharge; larger

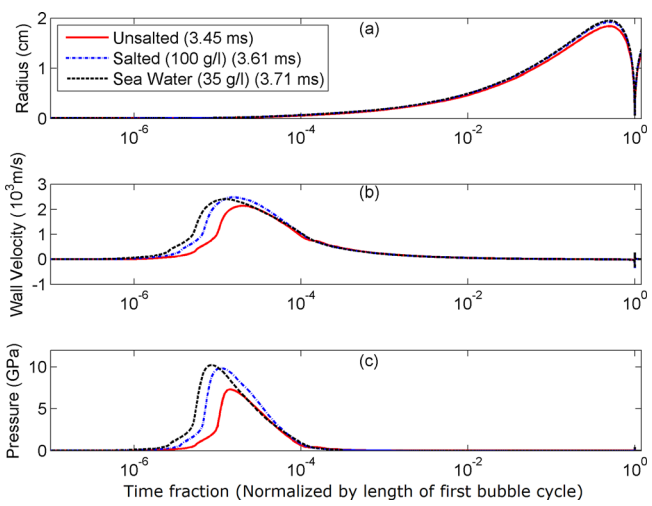

FIG. 5. Comparisons of (a) bubble growth and decay, (b) wall velocity, and (c) pressure as a function of time normalized by the first bubble period (shown in the legend) under different salinity conditions.

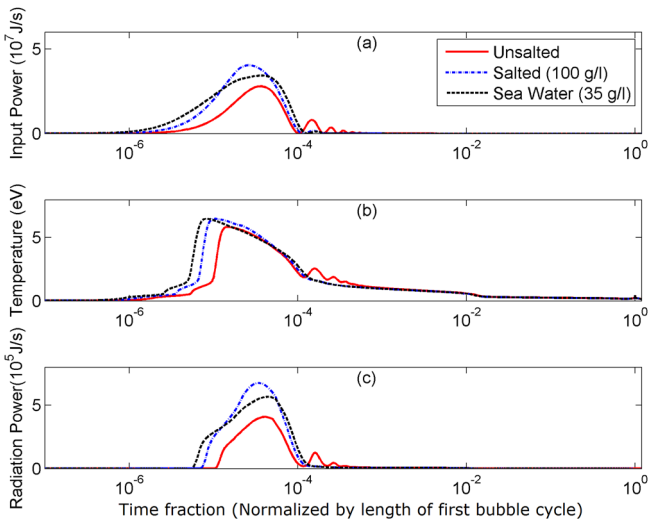

FIG. 6. Comparisons of (a) input power, (b) temperature, and (c) radiation power as a function of time normalized by the first bubble period under different salinity conditions.

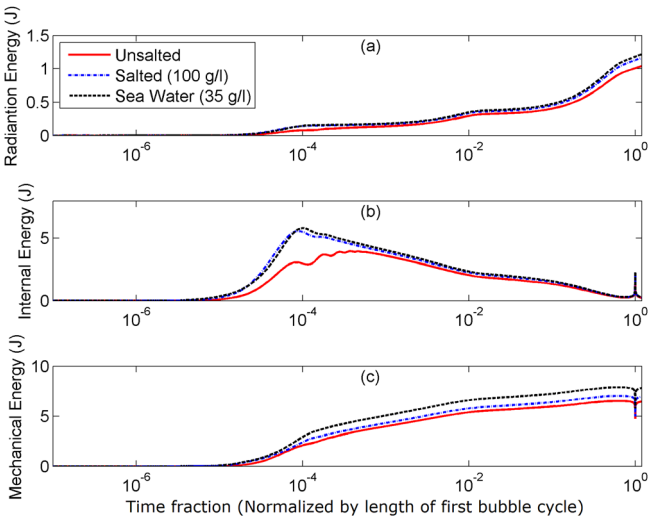

FIG. 7. Comparisons of (a) radiation energy, (b) internal energy, and (c) mechanical energy as a function of time normalized by the first bubble period under different salinity conditions.

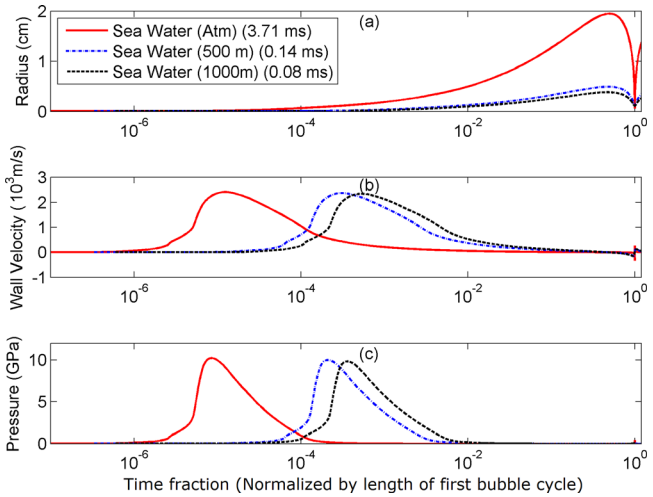

FIG. 8. Comparisons of (a) bubble growth and decay, (b) wall velocity, and (c) pressure as a function of time normalized by the first bubble period (shown in the legend) under different salinity conditions.

aperiodic curve of salted case indicates a critically damped discharge; while the wider aperiodic curve of seawater case indicates an over-damped discharge. Moreover, Fig. 6(a) also shows that the salted case requires the largest peak input power among these three cases. Temperature comparisons plotted in Fig. 6(b) show a sudden increase for all cases. The salted water case tends to have higher and earlier temperature rise. As shown in Eq. (21), radiation power is related to temperature and bubble surface area, the curves in Fig. 6(c) show combined trends from them.

Fig. 7 shows energy distribution during the first bubble cycle. Radiation energy curves plotted in Fig. 7(a) calculated by integrate radiation power along time. It shows that the salted and seawater cases lose similar amount of energy through the process, while the unsalted case loses slightly less. The internal energy (shown in Fig. 7(b)) difference in the beginning stage is due to the different input power curve. Since similar energy distributes into radiation loss and internal energy, the differences on mechanical energy is mainly due to the different amount of energy input into the gap.

The difference among atmospheric cases can be explained as follows: the total input energy to the gap can be calculated from simulation as 7.72 J (unsalted), 8.36 J (salted), and 9.28 J (seawater). Additionally, it is known that the circuit is under-damped in unsalted water, almost critically damped in salted water, and over-damped in seawater case. These differences lead to the fact that the input power of unsalted case is smaller but last periodically, the input power of salted case is higher and more intense, and the input power of seawater case starts earlier and last longer without periodic features. The earlier input power will be just used to heat smaller amount of particles in a smaller bubble, which results with higher temperature and pressure in seawater case. However, intense temperature peak in early stage emits less radiation energy due to smaller bubble surface area in salted case. Meanwhile, high pressure inside the bubble does more mechanical work during bubble expansion process in both salted and seawater cases. Since the internal energy and radiation energy are about the same at the end of first cycle, mechanical energy differences are mainly due to the difference of energy input to the water gap.

2. Ambient pressure study

The effect of different ambient pressures is also studied by simulating seawater spark discharge at different depths. Figs. 8–10 show the comparisons of all properties for all cases in seawater. Similarly, the time axis of each case is plotted in logarithmic scale and is normalized according to the first bubble oscillation cycle period. The cycle periods of all 3 cases are shown in the legend of Fig. 8(a) in parentheses.

Fig. 8(a) shows the comparison of radii for all seawater cases. It shows that the deeper the case locates, the smaller the bubble can expend and the shorter the first bubble cycle can last. Furthermore, apart from the radii comparison, other

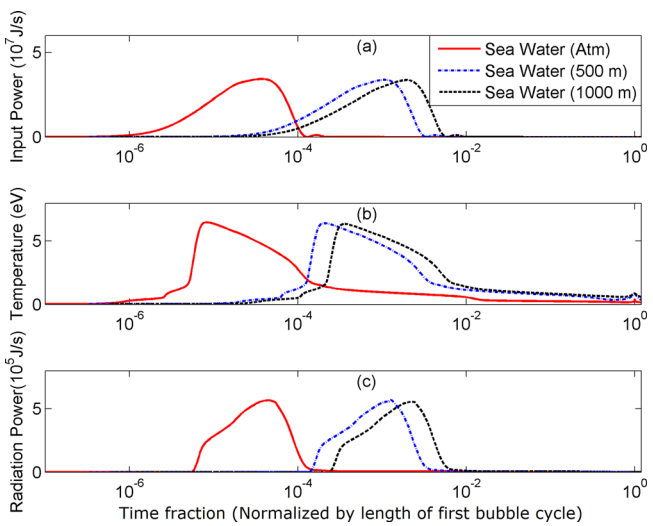

FIG. 9. Comparisons of (a) input power, (b) temperature, and (c) radiation power as a function of time normalized by the first bubble period under different ambient pressure conditions.

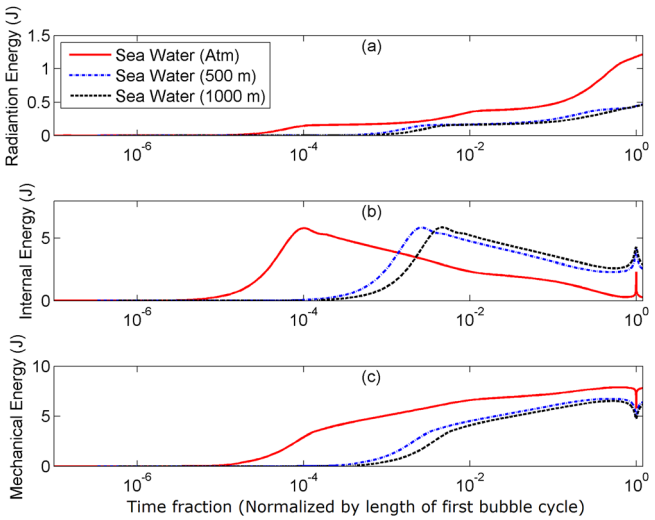

FIG. 10. Comparisons of (a) radiation energy, (b) internal energy, and (c) mechanical energy as a function of time normalized by the first bubble period under different ambient pressure conditions.

eight properties plotted in Figs. 8–10 show simple shifts in the time fraction axis for all three cases.

The study between different ambient pressure cases indicates that large ambient pressure prevents the vapor bubble from expanding to larger radius due to thermodynamic relations of pressure, temperature, and specific volume. This results in a smaller first bubble cycle. So, bubble properties like temperature, pressure, and system energy of deep ocean cases do not have enough time to develop as in atmospheric case.

3. Thermal radiation study

Fig. 11 shows a comparison of results obtained from (a) the black body radiation model and (b) a more realistic radiation model considering participating media. Smaller first bubble cycle periods are observed from the black body radiation model (a). Interestingly, despite showing different trends, two models have similar accumulative radiation energy levels after the first bubble cycle.

This can be explained by the fact that the smaller radiation rate leads to a smaller radiation heat loss at the beginning of the bubble cycle in model (b). Then, the temperature of vapor inside bubble will be higher than that of model (a) which results with higher radiation rate and longer first bubble cycle period when bubble expands and decays. Also, due to high voltage (~15 kV) and small capacitance in the case studied here, energy input rate is much higher than low voltage high capacitance underwater spark discharge. This results in higher temperature and higher particle density. So, radiation energy loss in this case is relatively higher.

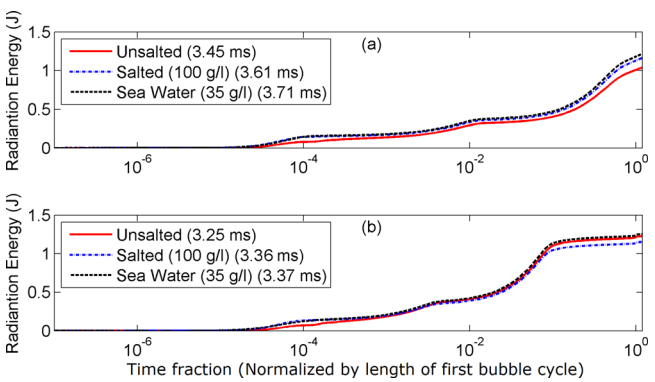

FIG. 11. Study of radiation energy using: (a) black body radiation and (b) participating media. Results are shown as a function of time normalized by the first bubble period (shown in the legend) under different salinity conditions.

IV. CONCLUSION

In summary, we introduced a new resistance model for spark discharge in dielectric and conductive liquids. We numerically investigated the bubble formation and oscillation processes created by underwater spark discharge in different salinity and different ambient pressure conditions. The different energy releasing mechanisms in conductive and dielectric liquids have been investigated. Additionally, spark discharge generating in deep ocean conditions was also simulated.

An experimentally validated bubble growth model was used for the bubble simulations. Although all simulations in this work showed periodic oscillation of bubbles, as the bubble grew in size its boundary become unstable causing random collapse during the process. This explains why there was no second bubble cycle detected in some cases.

We demonstrated that gap resistance in the circuit is the key difference between underwater sparks in dielectric liquid and in conductive liquid. After the spark gap switch is triggered, high voltage difference is applied on the electrodes. Afterwards difference discharging processes are initiated. In dielectric liquid (pure water), low resistance plasma channel connecting the electrodes is initiated by electrostatic repulsion and electrostriction force or the presence of a small bubble in the gap after a random latency period. Then, stored energy releases through the channel. In conductive liquid (salted water and seawater), stored energy releases directly through the current driven by high electric field in the conductive liquid which results in higher resistance. Furthermore, the gap resistance influences total energy release into the liquid and its damping characteristics. Specifically in conductive liquid, the larger total input energy for a single intense pulse shaped input power generates higher temperature, higher pressure, and higher bubble wall velocity. Therefore, more mechanical energy is released to surrounding liquid in comparison with dielectric liquid case. Hence, bubble generated by spark discharge in conductive liquid has larger pressure, no latency period, and does more mechanical work with the same energy consumed.

Ambient pressure is another parameter investigated in this work. Results from 500 m and 1000 m deep seawater simulations indicate smaller bubble radii and shorter bubble cycles in comparison with atmospheric seawater case. However, the maximum pressure and temperature within the bubble are nearly the same in both cases. Results suggest the underwater spark discharge process is applicable even in deep ocean conditions.

[1]E. O. Hulburt, Phys. Rev. **24**, 129–133 (1924).
[2]G. Cannelli, E. D'Ottavi, and A. Prosperetti, in *Proceedings of Oceans '90* (Washington, D.C., 1990), pp. 533–537.
[3]L. H. Fry, J. P. Adair, and R. Williams, in *Proceedings of 12th IEEE International Pulsed Power Conference* (Monterey, CA, 1999), Vol. 2, p. 781.
[4]J. S. Clements, M. Sato, and R. H. Davis, IEEE Trans. Ind. Appl. **IA-23**, 224 (1987).
[5]D. M. Willberg, P. S. Lang, R. H. Hochemer, A. Kratel, and M. R. Hoffmann, Environ. Sci. Technol. **30**, 2526–2534 (1996).
[6]M. Bourlion, P. Dancer, F. Lacoste, J. L. Mestas, and D. Cathignol, Rev. Sci. Instrum. **65**, 2356–2363 (1994).
[7]N. A. MacLeod, US Patent No. 3,180,418, April 27, 1965.
[8]Y. I. Cho, J. Lane, and W. Kim, Int. Commun. Heat Mass Transfer **32**, 861–871 (2005).
[9]Y. Yang, H. Kim, A. Starikovskiy, A. Fridman, and Y. I. Cho, Water Res. **44**, 3659–3668 (2010).
[10]B. R. Locke and S. M. Thagard, Plasma Chem. Plasma Process. **32**, 875–917 (2012).
[11]A. Starikovskiy, Plasma Sources Sci. Technol. **22**, 012001 (2013).
[12]G. N. Sankin, W. N. Simmons, S. L. Zhu, and P. Zhong, Phys. Rev. Lett. **95**, 034501 (2005).
[13]D. Obreschkow, P. Kobel, N. Dorsaz, A. de Bosset, C. Nicollier, and M. Farhat, Phys. Rev. Lett. **97**, 094502 (2006).
[14]K. Ando, A. Q. Liu, and C. D. Ohl, Phys. Rev. Lett. **109**, 044501 (2012).
[15]X. P. Lu, Y. Pan, K. F. Liu, M. H. Liu, and H. J. Zhang, J. Appl. Phys. **91**, 24–31 (2002).
[16]A. Grinenko, V. T. Gurovich, A. Saypin, S. Efimov, Y. E. Krasik, and V. I. Oreshkin, Phys. Rev. E **72**, 066401 (2005).
[17]N. Skoro, D. Maric, G. Malovic, W. G. Graham, and Z. L. Petrovic, Phys. Rev. E **84**, 055401(R) (2011).
[18]S. Buogo, J. Plocek, and K. Vokurka, Acta Acust. Acust. **95**, 46–59 (2009).
[19]J. A. Cook, A. M. Gleeson, R. M. Roberts, and R. L. Rogers, J. Acoust. Soc. Am. **101**, 1908–1920 (1997).
[20]P. Vanraes, A. Nikiforov, and C. Leys, J. Phys. D: Appl. Phys. **45**, 245206 (2012).
[21]M. S. Plesset and A. Prosperetti, Annu. Rev. Fluid Mech. **9**, 145–185 (1977).
[22]H. R. Griem, Phys. Rev. **131**, 1170 (1963).
[23]R. H. Cole, *Underwater Explosions* (Dover, New York, 1948).
[24]A. Prosperetti and A. Lezzi, J. Fluid Mech. **168**, 457–478 (1986).
[25]S. Fujikawa and T. Akamatsu, J. Fluid Mech. **97**, 481 (1980).
[26]E. V. Krivitski and V. V. Shamko, Sov. Phys.—Tech. Phys. **17**, 62–65 (1972).
[27]*The Sea*, edited by M. N. Hill (Wiley, New York, 1962), Vol. 1.